Available online at www.sciencedirect.com
SCIENCE DIRECT
Polymer 47 (2006) 390–402
polymer
www.elsevier.com/locate/polymer

Miscibility, crystallization and morphologies of syndiotactic polystyrene blends with isotactic polystyrene and with atactic polystyrene

Chi Wang *, Chang-Chun Lin, Lee-Chuan Tseng

Department of Chemical Engineering, National Cheng Kung University Tainan 70101, Taiwan, ROC

Received 10 June 2005; received in revised form 10 October 2005; accepted 23 October 2005
Available online 21 November 2005

Abstract

Two-component blends of differing polystyrene (PS), one syndiotactic (sPS) and the other isotactic (iPS) or atactic (aPS), were discussed. The phase behavior, crystallization and microstructure of binary polystyrene blends of sPS/iPS and sPS/aPS with a specific composition of 5/5 weight ratio were investigated using optical microscopy (OM), differential scanning calorimetry, wide-angle X-ray diffraction, scanning and transmission electron microscopy (SEM and TEM). Based on the kinetics of enthalpy recovery, complete miscibility was found for the sPS/aPS blends where a single recovery peak was obtained, whereas phase separation was concluded for the sPS/iPS blends due to the presence of an additional recovery shoulder indicating the heterogeneity in the molten state. These findings were consistent with OM and SEM observations; sPS/iPS exhibits the dual interconnectivity of phase-separated phases resulting from spinodal decomposition.

Both iPS and aPS have the same influence on the sPS crystal structure, i.e., dominant β-form sPS and mixed α-/β-form sPS obtained for melt-crystallization at high and low temperatures respectively, but imperfect α-form sPS developed when cold-crystallized at 175 °C. Co-crystallization of iPS and sPS into the common lattice was not observed regardless the thermal treatments, either cold or melt crystallization. Due to its slow process, crystallization of iPS was found to commence always after the completion of sPS crystallization in one-step crystallization kinetics. Segregation of rejected iPS component during sPS crystallization was extensively observed from TEM and SEM images which showed iPS pockets located between sPS lamellar stacks within spherulites, leading to the interfibrillar segregation, which was similar with that observed in the sPS/aPS blends. The addition of iPS (or aPS) component will reduce the overall crystallization rate of the sPS component and the retardation of crystal growth rates can be simply accounted by a dilution effect, keeping the surface nucleation intact. The phase-separated structure in the sPS/iPS blend shows a negligible effect on sPS crystallization and the signature of phase separation disappears after sPS crystallization. Depending on the relative dimensions of the segregated domains and iPS lamellar nucleus, subsequent crystallization of iPS can proceed to result in a crystalline/crystalline blend, or be inhibited to give a crystalline/amorphous blend morphology similar with that of sPS/aPS blends.

Keywords: Polystyrene blends; Crystallization kinetics; Blend morphology

1. Introduction

The stereochemistry of polymers plays an important role in determining the practical performance of polymers through a variety of thermal and morphological factors such as the glass transition, melting behavior and lamellar and spherulitic microstructure. Compared to its isomers, the recently-developed syndiotactic polystyrene (sPS) shows much promise as an engineering thermoplastics due to its high melting temperature and low dielectric constants. The widespread interest in this stereo-regular and crystallizable material has motivated many investigations on its conformation, configuration, crystal structure and crystallization kinetics to compensate the knowledge gap between its isotactic and atactic counterparts (iPS and aPS), which have been extensively studied in the past several decades. Improved polymer properties through blending with others continue to be an area of active industrial as well as academic concerns and ones of much intensive research effort. The miscibility of amorphous melt is strongly related to the stereochemical composition of the two components, e.g. short chain blends of atactic polypropylene (aPP) and isotactic polypropylene (iPP) are miscible in the melt but syndiotactic polypropylene (sPP) demixes from either iPP or aPP [1]. Miscibility of sPS and aPS in the melt state and the crystallization of this crystalline/amorphous blend have been already investigated previously [2–6]. However, there has been no literature yet reported on the

* Corresponding author. Tel.: +886 6 2757575x62645; fax: +886 6 2344496.
E-mail address: chiwang@mail.ncku.edu.tw (C. Wang).

0032-3861/$ - see front matter © 2005 Elsevier Ltd. All rights reserved.
doi:10.1016/j.polymer.2005.10.123

sPS/iPS system, which is believed to offer more varieties of microstructure interests due to its crystalline/crystalline blend characteristics. Mixtures of sPS and iPS should exhibit two distinct melting transitions, one for the sPS component located at ~ 270 °C, and the other for the iPS component at 220 °C. Moreover, by controlling the crystallization conditions for the sPS/iPS blends, either crystalline/crystalline or crystalline/amorphous structure can be obtained. It has been known that the introduction of diluents (either amorphous or crystalline) to crystallizable polymer chains is likely to change the morphology of mother polymer, leading to a drastic variation of apparent properties. Of particular interests are the location of the added diluent and its effect on the crystallization kinetics of the mother polymer.

Our work stems from a continuation of previous studies on the crystallization and morphology of sPS/aPS blends [7,8]. In these earlier works we were concerned with the crystallization of the sPS component from a homogeneous melt. Evidences for the complete mixing in the molten state and the crystallization-induced phase segregation were obtained from the thermograms and morphological micrographs. In this paper, we compare the phase behavior and crystallization kinetics of the sPS/aPS and sPS/iPS blends with a given composition of 5/5 weight ratio. With the same constituent monomer but different stereoregularities, these two athermal blends are good candidates for model studies to reveal the rigidity effects of the constituents on the blend miscibility and morphology, compared to the corresponding PP blends having relatively flexible backbone chains. Miscibility has been particularly studied using the enthalpy relaxation method via differential scanning calorimetry (DSC) as well as phase contrast microscopy. Effects of aPS (or iPS) on the crystallization of sPS and the developed morphologies, i.e. the crystal forms, lamellae, and spherulites, are discussed as well.

2. Experimental

2.1. Materials

sPS pellets with a weight-average molecular weight (M_w) of 200 kg/mol were obtained from Dow Chemical Co. The aPS and iPS samples were purchased from Aldrich Co. and Scientific Polymer Product Co., respectively. The characteristics of materials used are given in Table 1. Purification of the obtained iPS powder was conducted by the following procedure [11]: the amorphous iPS was first dissolved in boiling toluene, filtered, poured drop by drop into the large excess volume of methanol and then collected the precipitation. Continuous soxhlet extraction of the precipitated polymer was carried out with methylethylketone for 2 days and the residues were dried in vacuum. sPS blends were prepared by dissolving the calculated amount of individual components in *ortho*-dichlorobenzene (*o*-DCB) solvent at 140 °C to produce 1 wt% solutions. After 2 h thermal equilibrium in the oil bath, the homogeneous solution was then precipitated into a 20-fold excess volume of methanol. The precipitated powders were thoroughly washed with fresh methanol to remove residual *o*-DCB. Final drying of the precipitated polymer blend was accomplished by maintaining the samples under vacuum until constant weights. sPS/aPS and sPS/iPS blends with a 5/5 weight ratio were prepared. The as-prepared blend powders were completely amorphous based on their wide-angle X-ray diffraction (WAXD) patterns where only amorphous halo was observed.

Table 1
Characteristics of polystyrene used

	T_g (°C)	T_m^0 (°C)	M_w
sPS	95	291[a]	200k
iPS	90	240[b]	400k
aPS	99	–	100k

[a] Obtained from Ref. [9].
[b] Obtained from Ref. [10].

2.2. Analytical techniques

Thermal events of the sPS blends were measured using a Perkin–Elmer DSC7 with a heating rate of 10 °C/min under nitrogen atmosphere. The crystal growth rates (G) were measured using a polarized optical microscope (POM, Leica, DMLP) equipped with a thermal hot stage (Linkam, THMS600) for temperature control. Prior to measurements, the hot stage was calibrated with benzoic acid. By measuring the light-intensity variation under the microscope with cross-polars configuration, transmitted light intensities during crystallization were recorded by an AP1 camera (Apogee Instruments Inc.) to monitor the crystallization kinetics for various thermal treatments on the blends, either one-step or two-step crystallization. The details of the experimental setup were described in ref. 12. One-step melt-crystallization was conducted by cooling the samples from 300 °C rapidly (100 °C/min) to the given crystallization temperature (T_c) for allowing the crystallizable component to crystallize. On the other hand, one-step cold-crystallization was performed by heating the amorphous blends rapidly (100 °C/min) from room temperature to the desired T_c. For two-step crystallization, the sPS/iPS blend was first cooled to a desired T_c (which is higher than melting point of iPS, ~ 220 °C) to commence crystallization of sPS for a sufficient period; then the blend was rapidly cooled to a lower T_c at which crystallization of iPS was likely to proceed. Melting behavior of the crystallized blends was observed under POM at a heating rate of 10 °C/min as well.

WAXD patterns of the crystallized samples were obtained using a Rigaku (Dmax2000, Cu target) X-ray diffractometer to characterize the crystal lattice. Thin sections of sPS blends, stained with ruthenium tetraoxide vapors, were used and observed with a TEM (Jeol, JEM-1200EX) microscope. Morphology of the lamellar stacks of sPS blends was also observed using SEM (Hitachi, S4100). Prior to SEM observation, the crystallized blends were etched using amyl acetate to extract the aPS (or amorphous iPS) component. The etching procedure followed the method proposed by Kit and

Schultz [13]. Fourier transform infrared (FTIR) spectra were recorded with a Jasco model 460 FTIR Spectrometer.

3. Results and discussion

3.1. Miscibility studies

3.1.1. Enthalpy relaxation

Accordingly to the conventional DSC measurements, a blend is often regarded as being miscible when it exhibits a single glass transition temperature and immiscible (or partially miscible) when two distinct T_gs are detected. However, above deduction can only apply to the system where the T_gs of the pure components are sufficiently far apart. Since T_gs of PS with different tacticities are rather close to one another (Table 1, $\Delta T_g < 10$ °C), the above single T_g criterion is not applicable to determine the miscibility of PS pairs. However, the enthalpy relaxation study by DSC annealing at a temperature below T_g is an appropriate approach to reveal phase behavior of the constituent polymers [14,15]. Enthalpy relaxation process involves the change of enthalpy of a glass polymer from its initial thermodynamic nonequilibrium state towards its final equilibrium state. Upon annealing a glassy blend for a long period of time at a temperature lower than its T_g for prohibiting the long range motion, the enthalpy of the blend is decreased as a function of time due to the segmental motions of long chains. During the subsequent heating trace, the loss of enthalpy will be recovered as a pronounced endothermic (ageing) peak in most cases. Based on the fact that each polymer has its own enthalpy relaxation kinetics, a miscible blend will give a single enthalpy recovery peak, whereas two recovery peaks implies that phase separation has taken place before annealing, leading to the presence of two relaxation mechanisms to follow. Thus, judging from the position and magnitude of the enthalpy recovery peaks, the polymer–polymer miscibility can be revealed.

Fig. 1 shows the DSC heating traces of sPS/iPS blends after being annealed at 75 °C for various time (t_a). Prior to annealing, the samples were held at 300 °C for 10 min and then quenched to liquid nitrogen to freeze the morphology developed. Without annealing, only one incremental change in specific heat is identified, due obviously to the similar T_g values of sPS and iPS. After annealing for 12 h, an enthalpy recovery peak at 92.1 °C together with a discernible shoulder at 99.8 °C can be seen. For longer annealing, the enthalpy recovery peaks become more pronounced. After 48 h annealing, the samples exhibit a significant endothermic peak at 96.7 °C and discernable shoulder at ca. 100.9 °C, suggesting the presence of two different phases within samples. It is suspected that sPS/iPS = 5/5 blends become phase-separated at 300 °C and an upper critical dissolution temperature (UCST) phase boundary might exist. To estimate the UCST temperature, experiments were conducted on the blend at a melt temperature of 320 °C but similar enthalpy recovery behavior was obtained. Higher temperature experiments are infeasible since the degradation of PS becomes pronounced at ca. 340 °C according to our thermo-gravity analysis.

Fig. 2 shows the DSC heating traces of melt-quenched samples after being annealed at 75 °C for 48 h. In contrast with the sPS/iPS blend, the presence of a single pronounced endothermic peak is evident for the sPS/aPS blend, indicating the formation of miscible blend which is consistent with previous reports [2–5]. The recovery peak temperatures for the neat components are: 104.9 for aPS, 100.7 for iPS, 101.4 for sPS, and 101.2 °C for the sPS/aPS blend. In addition, the neat sPS and iPS exhibit crystallization exotherms with peak temperatures centered at 149.2 and 186.2 °C, respectively, as shown in Fig. 2. For the sPS/aPS blend, the crystallization peak is shifted to 162.3 °C due mainly to the dilution effect. For the sPS/iPS blend, on the other hand, two crystallization peaks associated with the sPS component occur at 139.9 (major) and 153.2 °C (minor) due to the plausible presence of two phases and the enhanced mobility upon addition of iPS, which has a lower T_g compared with that of sPS (Table 1). As shown in Fig. 1, the minor crystallization exotherm is more discernible when the heterogeneity within samples is enhanced effectively by long-period annealing. To verify that the observed

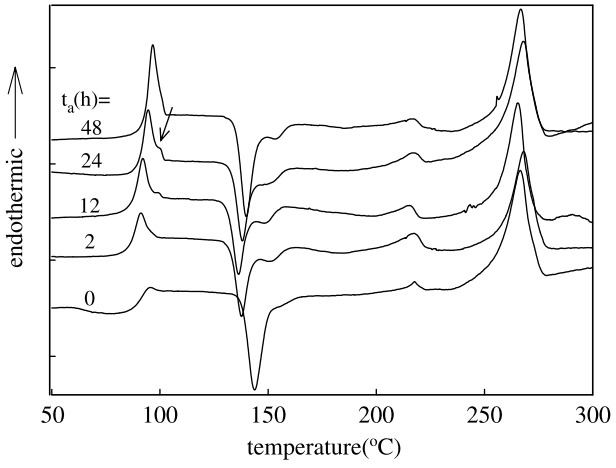

Fig. 1. DSC heating traces for melt-quenched sPS/iPS blends annealed at 75 °C for various times t_a.

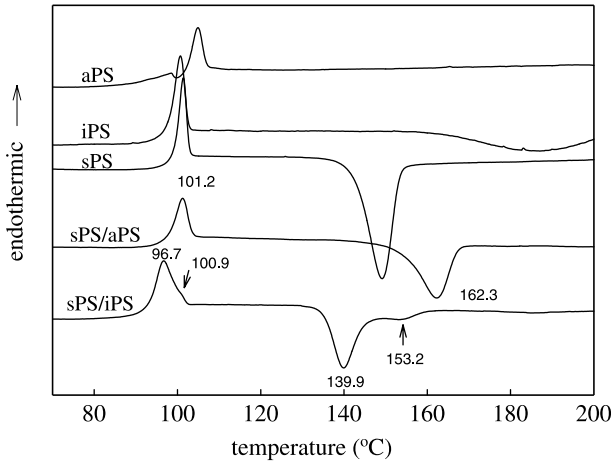

Fig. 2. DSC heating traces for samples annealed at 75 °C for 48 h. Prior to annealing, the samples were held at 300 °C for 10 min and then rapidly quenched to preserve the phase structure of the molten state.

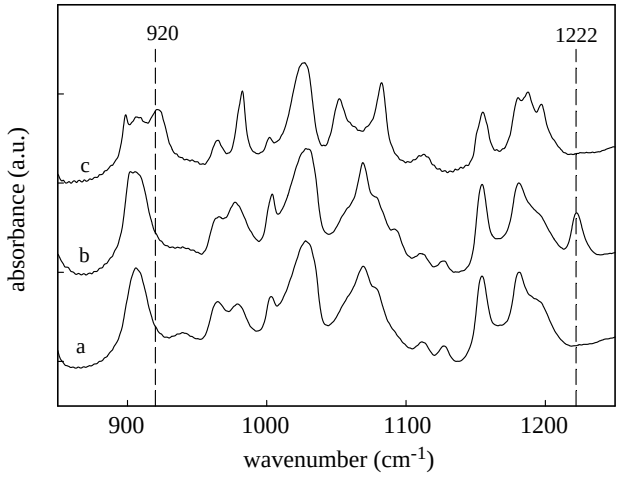

Fig. 3. FTIR results for sPS/iPS = 5/5 blends to justify the absence of iPS crystallization at T_c lower than 160 °C, supporting that both crystallization exotherms in Fig. 1 are associated exclusively with the sPS component in the sPS-rich and iPS-rich domains, respectively. Curve a: amorphous blend, b: heating the amorphous blend to 160 °C and then quenched, and c: crystallized neat iPS.

exotherms are exclusively associated with the cold crystallization of sPS, not the iPS as well, FTIR spectroscopy was conducted on the sPS/iPS blends which were heated to 160 °C and quenched rapidly in liquid nitrogen. As shown in Fig. 3, the absorbance bands at 899 and 920 cm^{-1} [16] which are characteristic of the iPS crystallites are not observed, whereas the 1222 cm^{-1} band [17] which is relevant to the sPS chains possessing the planar zig-zag conformation in the crystalline region is observed. Moreover, it is of interest to note that the crystallization peak for iPS component at ~186 °C is barely seen in the sPS/iPS blend (Fig. 1) because of its low crystallization rate, which is consistent with the results obtained from the isothermal crystallization studies (discussed later).

3.1.2. OM and SEM observations

Due to the structure similarity, the refractive indexes of PS with different taciticity are rather close each other, leading to the difficulty in studying the liquid–liquid phase boundary of the binary blends in situ using cloud-point method (either by light scattering or optical microscopy) based on the turbidity measurement. However, it was found that enhanced phase contrast for melt-quenched samples can be obtained under phase contrast microscopy. Thus, the blend samples were held at 300 °C for various times (t_a) and then rapidly quenched into liquid nitrogen to preserve the morphological features developed. Based on the assumption that the phase structure is preserved on rapid quenching, the structural development for sPS/iPS blends is shown in Fig. 4 which exhibits apparent

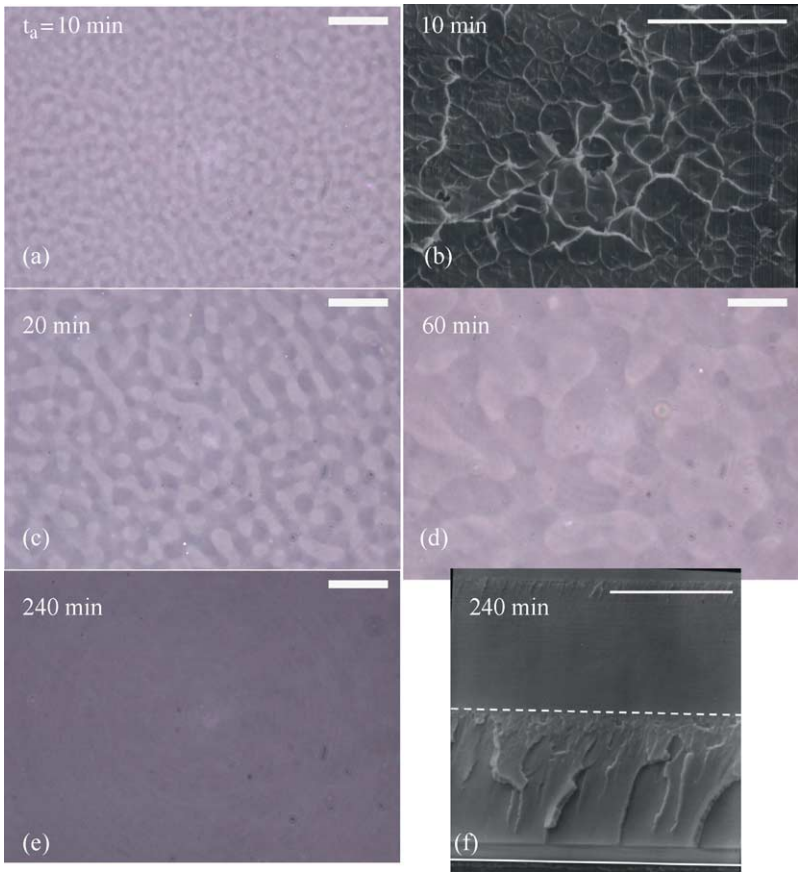

Fig. 4. (a,c,d,e) Phase-contrast optical micrographs of time development surface pattern associated with the phase separation of sPS/iPS = 5/5 films after melt quenching from 300 °C, at which samples are held for various periods t_a, (b, f) SEM images of the sample obtained in the thickness direction. The dashed line in (f) indicates the boundary of the two layers with different morphological features. Scale bar: 20 μm.

phase separation morphology; whereas featureless structure is obtained for the sPS/aPS blends (not shown here for brevity), indicating homogeneous and miscible state at 300 °C. The darker region is the sPS-rich phase and the lighter region is the iPS-rich phase. To reveal the blend structure with fine resolutions, SEM is also a powerful tool to identify the plausible presence of any phase separation event, if exists, on the basis of distinct domain variation. As given in Fig. 4(b) and (f) are the SEM images for sPS/iPS blends experienced a residence time of t_a at 300 °C prior to liquid-nitrogen quenching. The OM images were obtained from the through view of the samples, whereas SEM images were obtained from the edge view (thickness direction). Based on the OM and SEM images, the characteristic features of the morphology are regular, with a periodic wavelength, and dual interconnected phases (sPS-rich and iPS-rich domains). The interconnected domains, however, do not give rise to the typical ring pattern in the Vv light scattering mode as always being found in the phase-separated blend systems, indicating the weak scattering intensity, which might be obscured by the relatively strong background scattering. Instead, two-dimensional fast Fourier transforms (FFT) of the OM micrographs were conducted and the periodic wavelengths of the modulated structure were obtained from the spinodal rings. The periodic wavelength increases with increasing t_a, suggesting the coarsening process of the spindoal decomposition. It is of importance to note that the phase-separated structure disappear for samples annealing for a longer period (t_a larger than 150 min). This phenomena can be attributed to two facts; the first is the density difference between the sPS-rich and iPS-rich phases and the second is relevant to the low viscosity of the blends at such a high temperature (300 °C). For the coarsening process of spinodal decomposition, it is well-known that the main driving force is the ratio of the interfacial energy and the viscosity of the blends. At 300 °C, the melt viscosity of the blends is sufficiently low and a significant high coarsening rate of 0.32 μm/min is obtained from the linear slope of the periodic wavelength vs. t_a plot. It has been pointed out that sPS chains are more likely to take the trans conformation in the glassy state [18]. Hence, at a given molecular weight sPS exhibits a larger radius of gyration and possess a lower density than iPS. Thus, during the coarsening process, the sPS-rich domains having a relatively lower density will float upwards to form an upper layer in the blend film. On the other hand, iPS-rich domains will gradually move downwards to develop a bottom layer. At the final stage of phase separation, a double layer structure is evidently developed as observed by SEM from the edge view (Fig. 4(f)) but featureless structure obtained by OM from the through view (Fig. 4(e)). According to Fig. 4(f), it also implies that the amount of the sPS-rich domains (upper layer) are higher than the iPS-rich domains (bottom layer), suggesting that the minor cold-crystallization peak (Fig. 1) is associated with the crystallization of the sPS component in the iPS-rich domains.

Accordingly, the morphological evolution of the blend in the melt state evidently implies that sPS/iPS is undergoing a process of liquid–liquid demixing at 300 °C. The appearance of the bicontinuous domain structure suggests that the liquid–liquid demixing occurs by a process of spinodal decomposition flowed by the coarsening process. At 320 °C, spinodal decomposition morphology of sPS/iPS blends is still discernible but the coarsening rate is increased since the blend viscosity is further reduced. It is in good agreement with enthalpy relaxation results (Fig. 1), showing two different relaxation mechanisms and cold-crystallization kinetics in the phase-separated blend (i.e. sPS-rich and iPS-rich domains, respectively). In contrast, miscibility of sPS/aPS blends is further verified on the basis of OM and SEM images since homogeneous structure without any particular features is obtained, consistent with previous enthalpy relaxation results (Fig. 2). For the sPS/iPS blends, the miscibility gap and the phase diagram are currently being studied using samples with different compositions. The detailed results will be provided in a future article.

The foregoing paragraphs identify the miscibility of PS melts in which the chains differ merely in stereochemical compositions. Our findings in PS blend system are quite similar with those in the PP blend system, i.e. the sPP/iPP system is more immiscible than the sPP/aPP system [1]. To realize the reasons to account for the better mixing of sPS with aPS, as compare to sPS with iPS, one has to take the conformation of individual chains into consideration. On studying the chain conformations of glassy PS using solid state high resolution ^{13}C NMR, Nakaoki and Kobayashi [18] quantitatively determine the gauche content of each stereo-isomer: 25.0, 27.9 and 34.3% for sPS, aPS and iPS, respectively. These results imply that the sPS chains prefer trans sequences and the iPS chains are the least to take trans sequences among them. The similar tendency for sPS and aPS chains to possess trans sequence conformation might lead to a better miscibility. However, iPS chains are more likely to take the gauche conformation that is difficult to match and interact with the conformational structure of sPS. Thus, when iPS chains are included, the disruption of the attractive interactions caused by co-operative trans sequences in the sPS melt might take place and demixing occurs to form a phase-separated structure. However, a detailed conformational analysis of PS chains must be carried out by molecular dynamics simulation before a sequence interaction can be proposed to reveal the detailed miscibility results.

3.2. One-step crystallization of sPS/iPS

Fig. 5(a) shows the crystallization isotherms for samples crystallized at 175 °C for a time period long enough to conclude the crystallization. $I(t)$ and I_{max} are the light intensity at time t and the saturated intensity measured by the Apogee camera under POM with cross polars. The normalized intensity, $I(t)/I_{max}$, is used to represent the relative crystallinity during structural evolution [12]. The WAXD patterns of the crystallized samples are displayed in Fig. 5(b) for determining the crystal form developed.

As shown in Fig. 5(a), the transmitted light for the neat sPS is increased abruptly within a short period, suggesting the fast

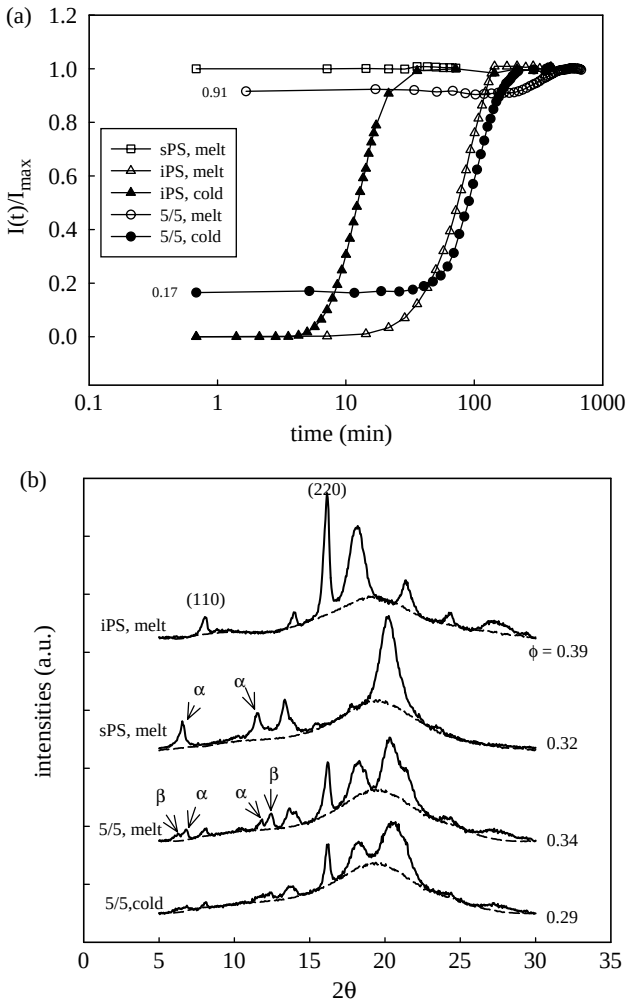

Fig. 5. One-step crystallization of samples crystallized at 175 °C either from the melt or glassy state. (a) Time evolution of transmitted light intensities of samples during crystallization observed under POM, (b) WAXD patterns of the crystallized samples; the dashed lines are intensities contributed from the amorphous phase.

crystallization of sPS at 175 °C. On the other hand, a sigmoidal time dependence of $I(t)/I_{max}$ is observed for neat iPS melt-crystallized at 175 °C. The crystallization half-time, $t_{1/2}$, defined as the time required to achieve 50% of the normalized crystallinity was determined to be 67.7 min for the neat iPS, indicating a much lower crystallization rate of iPS compared to sPS. Also given in Fig. 5(a) is the crystallization curve for iPS cold-crystallized at 175 °C, which gives a $t_{1/2}$ value of 8.3 min. The decrease in the crystallization half-time is indicative of the enhanced crystallization rate, which is attributed to a rapid nucleation process involved in the cold crystallization.

For sPS/iPS blends, melt-crystallization of sPS component is completed in a short period and a constant $I(t)/I_{max}$ is quickly reached at ~0.91, followed by the slow increase of $I(t)/I_{max}$ associated with the crystallization of iPS component. Under POM observations, it was found that sPS crystallized and filled the whole space before the set T_c (175 °C) was reached even at the fastest heating (or cooling) rate 100 °C/min, indicating that sPS and iPS crystallize sequentially and not simultaneously. Moreover, the fact that sPS spherulites are space-filling indicates that iPS is rejected as a non-crystallizable component and reside primarily in the interfibrillar regions of the sPS spherulites (discussed later). Subsequent crystallization of iPS takes place within the sPS spherulites. It is also of interest to note that when melt-crystallized, majority of the crystals are relevant to the sPS component based on the high $I(t)/I_{max}$ level induced by sPS; the rest being associated with iPS. In contrast, the fraction of sPS crystals contributing to the transmitted intensities is reduced to ~0.17 when cold crystallization is conducted. Compared to neat iPS, moreover, crystallization of iPS in the blends is significantly hindered on the basis of the derived $t_{1/2}$ values, being 66.6 and 89.7 min for cold- and melt-crystallization, respectively. To account for the crystallization kinetics, the Avrami equation is frequently used to derive the rate constant (k) and the dimensionality of growth (n),

$$v(t) = \frac{I(t)}{I_{max}} = 1 - e^{-k(t-t_0)^n} \quad (1)$$

where t_0 and $v(t)$ are the induction time and the volume transformation at time t from the liquid to crystals. As given in Table 2 are the values of k and n derived, respectively, from the intercept and slope by plotting the curve of $-\ln[\ln(1-v(t))]$ vs. $\ln t$. For neat iPS, the deduced k value for cold crystallization is about two orders of magnitude higher than that for melt crystallization. For the iPS component in the blends, however, comparable crystallization rates are obtained for cold and melt crystallization but their values are reduced due to the addition of sPS. Thus, crystallization of iPS from the glassy or molten state is retarded by the presence of sPS. The nucleation mechanism and crystal geometry of iPS phase is hardly affected by the presence of sPS since a constant exponent (~2.0) is obtained in the neat state as well as in the blends. As shown in Fig. 5(a), it is also worthwhile to note that the induction time is also significantly increased in the blends.

According to the WAXD profiles as shown in Fig. 5(b), co-crystallization of sPS and iPS is not observed when the blend samples are crystallized at 175 °C either from the melt or from the glassy state. The absence of co-crystallization can be realized due to the large differences in the crystallization rate and crystal lattices as well as the wide separation of crystallization regimes. The diffraction peaks at $2\theta \sim 7.9$ and 16.1° corresponding to the (110) and (220) diffraction planes of iPS are used to identify the presence of the iPS crystallites [16]. The crystal lattices of iPS remain intact (hexagonal lattice with $a = 2.19$ and $c = 0.67$ nm) in spite of sPS incorporation, whereas different forms of sPS crystals are developed due to its polymorphic nature [19–21]. Two crystalline structures, i.e.

Table 2
One-step crystallization data for the iPS component at 175 °C in the neat and blend samples

	Neat iPS		iPS in the blends	
	k (min^{-1})	n	k (min^{-1})	n
Cold crystallization	1.73×10^{-2}	1.7	3.61×10^{-5}	2.3
Melt crystallization	1.75×10^{-4}	2.0	2.67×10^{-5}	2.1

the hexagonal α form ($a=2.63$, $c=0.51$ nm) and orthorhombic β form ($a=0.88$, $b=2.88$, $c=0.51$ nm), are generally obtained for sPS crystallization without the presence of solvents used [19]. Several factors, e.g. the holding temperature of the melt, the crystallization temperature, and the cooling rate, are important in determining the crystalline structure of sPS. Guerra et al. [19] and Woo et al. [21] gave a detailed analysis of the conditions leading to different crystal forms of sPS. In general, development of the α form is favored under the crystallizations conditions of (i) low holding temperature, (ii) fast cooling from the melt, (iii) melt crystallization at low temperatures, and (iii) cold crystallization from the glassy state [19,21–26]. As shown in Fig. 5(b), only α-form crystallites are detected for neat sPS melt-crystallized at 175 °C, which is consistent with previous findings by Bu et al [22] who found that pure α-form sPS was developed at 170 °C. Due to the high cooling rate (100 °C/min) as well as the low crystallization temperature (175 °C) used here, the absence of the β form is not unexpected. When melt-crystallization of sPS/iPS is conducted at 175 °C, on the other hand, characteristics of iPS peaks are evident but sPS is crystallized into mixed crystals, containing the α form with characteristic peaks at $2\theta\sim6.8$ and 11.7° as well as the β form corresponding at $2\theta\sim6.2$ and 12.3°. Hence, addition of iPS favors the development of the β-form crystallites of sPS, which is similar with the sPS/aPS blends [4,5,24].

For sPS/iPS samples crystallized from the glass, in contrast, the plausible transformation of the mesomorphic phase to barely-observed -form sPS is recognized due to the presence of broad peaks at $2\theta\sim7$ and 12°. For neat sPS, the same crystalline structure has been reported previously [27]. Sample crystallinity (ϕ) was determined from the area ratio of the diffraction peak to the total scattering. The contribution of the amorphous phase to the WAXD patterns is shown by the dashed line. It is found that the crystallinity of sPS/iPS samples crystallized from the glassy state is slightly lower than that crystallized from the melt plausibly due to the crystal imperfection.

3.3. Two-step crystallization of sPS/iPS—(T_{c1}/175 °C)

Fig. 6(a) shows the crystallization curves of sPS/iPS crystallized first at $T_{c1}=241$, 250 or 262 °C and then rapidly cooled to 175 °C, where subsequent crystallization of iPS proceeds. The effect of iPS addition on the crystallization of sPS component at the first step (T_{c1}) was studied. Moreover, it was expected that iPS chains were expelled from the sPS crystal growing front to form segregated domains, whose sizes might be dependent upon T_{c1}. Thus, crystallization of iPS in these confined domains at the second step (175 °C) was also investigated. Melting behavior of the crystallized blends was also traced by the intensity variation during subsequent heating at a rate of 10 °C/min to 300 °C. To eveal the melting temperatures, the derivative of the transmitted light intensities [12] was used as shown in Fig. 6(b). The two melting peaks at temperature below 240 °C are associated with the iPS crystal melting, whereas the melting peaks above 240 °C are attributed

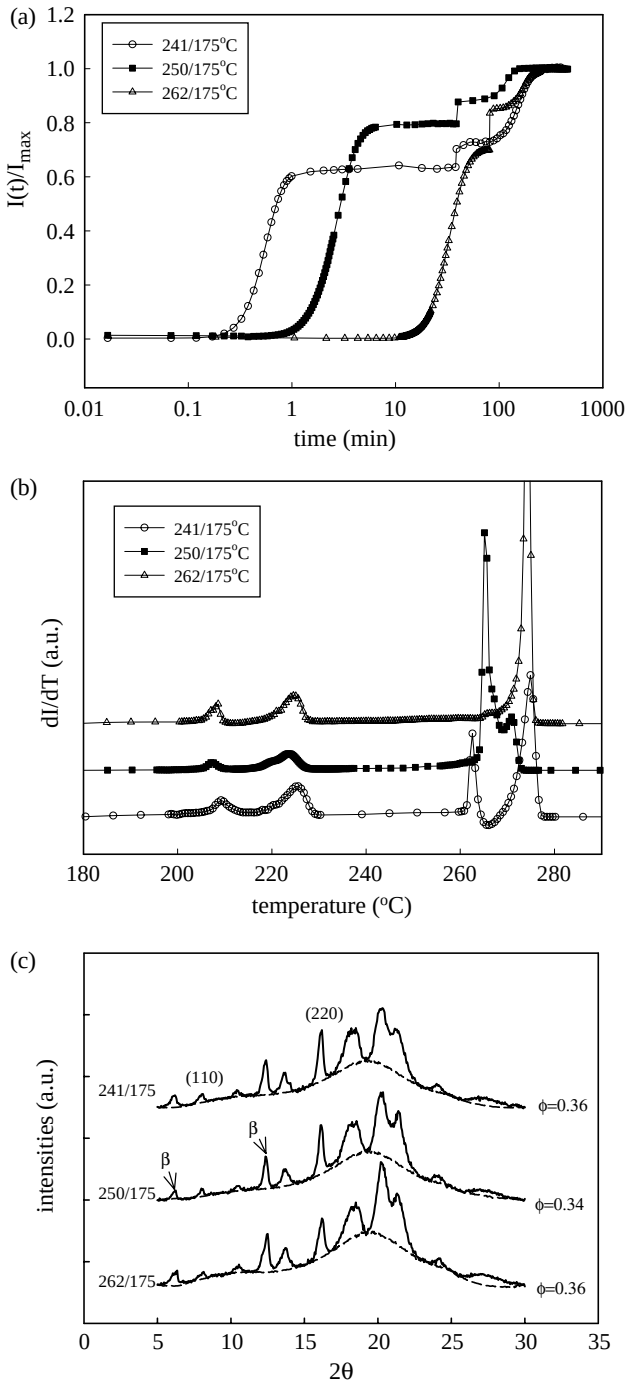

Fig. 6. Two-step crystallization of samples crystallized first at 241, 250 or 262 °C to complete sPS crystallization and then cooled to 175 °C for iPS crystallization to proceed. (a) Time evolution of transmitted light intensities of samples during crystallization observed under POM, (b) melting behavior of samples observed under POM, (c) WAXD patterns of the crystallized samples, ϕ denoting the overall crystallinity.

to the sPS crystal melting. Fig. 6(c) gives the WAXD patterns of the crystallized blends.

For this two-step crystallization process, it is evident that separate crystallization kinetics is exhibited individually for the sPS and iPS components due to the presence of step-wise increases in the transmitted light intensities, Fig. 6(a). The

initial increase of intensities is associated with the sPS crystallization at T_{c1} and the final intensities rise is relevant to the iPS crystallization at 175 °C. However, it is intriguing to note the presence of abrupt intensity jump immediately right after the temperature is changed from T_{c1} to 175 °C. It suggests that small amount of sPS in the iPS-rich domains do not crystallize at T_{c1} but become crystallizable at a somewhat lower temperature, in accord with Fig. 1.

For the sPS in the blends, $t_{1/2}$ values are 0.7, 3.0 and 38.9 min, respectively, for the two-step crystallization occurring at $T_{c1}=241$, 250 and 262 °C. The derived $t_{1/2}$ values for neat sPS crystallized at 241, 250 and 262 °C are 0.4, 1.7 and 24.6 min, respectively (the graphs are not shown here for brevity). As expected, the crystallization rate of sPS is higher at a lower T_{c1} and crystallization rate of sPS is retarded by the iPS addition because of a larger $t_{1/2}$ required for the blend. Table 3 displays the Avrami exponents and the crystallization rate constants derived from the Avrami plots. The addition of iPS does not affect the n value of sPS kinetics, but the crystallization rate of sPS in the blend is decreased at all T_{c1} studied. Regardless of the previous T_{c1} used for sPS crystallization, a similar kinetics is obtained for the subsequent crystallization of iPS at 175 °C, suggesting that the size of segregated iPS domains plays a negligible effect on the subsequent iPS crystallization within these regions. Indeed, similar dimensions of segregated domains are observed under SEM (Fig. 10). The k value for iPS crystallization in this two-step process is 8.48×10^{-5} min^{-1}, which is lower than that for the neat iPS, but larger than that obtained from the one-step crystallization process (Table 2).

As seen in Fig. 6(b), the melting behavior of iPS remains essentially unaffected by the presence of sPS component, indicating that the lamellar thickness, which is known to determine the melting temperature of the crystallites, is independent of T_{c1}. These two T_m are identical to those of neat iPS crystallized at 175 °C. The double melting behavior of iPS is due to the presence of two distinct lamellar components with different thermal stabilities within a single lamella [28]. The less perfect lamellar domains melt first at the lower temperature, while the higher melting peak is due to the melting of more perfect part within the same lamella as well as the melting of re-crystallized population during the heating process. Since our melting curves are obtained on the basis of the variations of transmitted light intensities due to the spherulitic melting, the annealing peak associated with the melting of the rigid amorphous phase, which is frequently observed using infrared spectroscopy and DSC [16,28], seems too subtle to be resolved.

Table 3
Two-step melt-crystallization data for the sPS component in sPS/iPS blends at T_{c1}/175 °C, together with results of the neat sPS at T_{c1}

T_{c1} (°C)	sPS in the blends		Neat sPS	
	k (min^{-1})	n	k (min^{-1})	n
241	5.47	2.4	9.42	2.5
250	0.11	2.3	0.48	2.2
262	5.04×10^{-4}	2.3	7.29×10^{-4}	2.4

iPS in the blends: $k=8.48\times10^{-5}$ min^{-1}, $n=2.3$ at 175 °C.

Regarding the sPS component, two melting peaks at 262.6 and 274.5 °C with a shallow recrystallization peak at 266.1 °C are identified for $T_{c1}=241$ °C, suggesting the occurrence of the melting-recrystallization-remelting phenomena during the heating scan [5]. Double melting peaks are also observed for $T_{c1}=250$ °C where a pronounced melting peak located at 265.1 °C, accompanying with a small shoulder at 270.9 °C. Crystallized at higher T_c (262 °C), sPS crystallites become more perfect and a single melting temperature at 274.5 °C is observed. In addition, the melting behavior and melting temperatures of the blends are similar with those found for the neat sPS. In contrast with melt-crystallization at 175 °C where coexistence of the α and β form sPS is concluded (Fig. 5(b)), sPS/iPS blends exhibit only the β-form sPS at higher temperatures as shown in Fig. 6(c). A similar trend was also observed in that the 250 °C melt-crystallized sPS/aPS blend exhibits the β-form sPS only [7,24]. Thus, the addition of either iPS or aPS essentially favors the formation of the β form and reduces the possibility of the α form developing, eventually giving rise to the pure β form at temperatures higher than 240 °C. The crystallinity fraction of blends is independent of T_c and is about 0.35, being the weight average of the neat components.

3.4. Two-step crystallization of sPS/iPS—(250/T_{c2} °C)

To study the iPS crystallization kinetics in controlled confined regions, two step-crystallization was carried out at 250/150, 250/175 and 250/200 °C, respectively. Fig. 7(a) displays the crystallization curves and the WAXD intensity profiles of the crystallized samples are shown in Fig. 7(b).

Similar with previous results (Fig. 6(a)), an abrupt increase of transmitted intensities is observed when the temperature is quickly changed from 250 °C to T_{c2}, suggesting the existence of some sPS chains which are unable to crystallize at 250 °C but become crystallizable at a lower temperature. This unique feature is attributed to the phase-separated structure of the blends and the sudden increase of sPS crystallites is relevant to the crystallization of sPS in the iPS-rich domains. As shown in the 250/150 and 250/175 °C processes, after a certain induction time the crystallization of iPS gives rise to the sigmoidal intensity increase. In the case of 250/200 °C, however, it is readily noted that the crystallization and the subsequent melting behavior associated with iPS component are not observed. It seems that crystallization of iPS at 200 °C is inhibited in the confined segregated domains with a width of ~160 nm (Fig. 10(b)). In contrast, the crystallization event of iPS is evidently seen in 250/150 and 250/175 °C cases and the derived Avrami parameters are tabulated in Table 4, together with those for neat iPS. The reduction of iPS crystallization rates upon addition of sPS is evidently revealed.

For sPS/iPS blends melt-crystallized at 250 °C first and then quenched to room temperature to prohibit iPS crystallization, it leads to the development of sPS crystals in the β form exclusively (not shown here), which is similar with that for

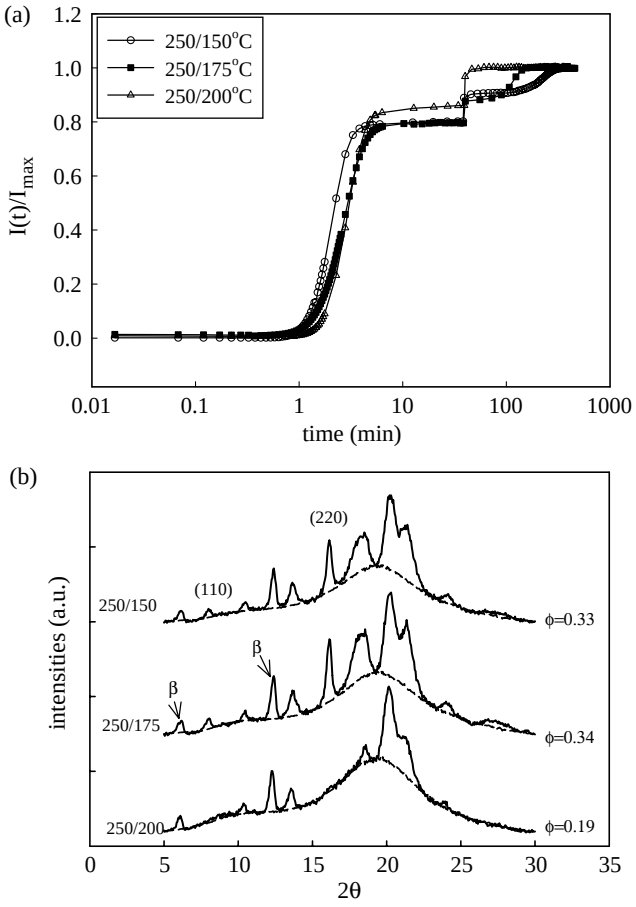

Fig. 7. Two-step crystallization of samples crystallized first at 250 °C to complete sPS crystallization and then cooled to 150, 175, or 200 °C for iPS crystallization to proceed. (a) Time evolution of transmitted light intensities of samples during crystallization observed under POM, (b) WAXD patterns of the crystallized samples, ϕ denoting the overall crystallinity.

sPS/aPS blends [7,24]. For 250/175 °C two-step crystallization, diffraction peaks contributed from iPS crystals and sPS crystals in the β form are seen in Fig. 7(b). Similar WAXD pattern can be observed for the blend conducted by 250/150 °C two-step crystallization. For 250/200 °C two-step crystallization, however, it is intriguing to note that only the WAXD peaks associated with sPS are present but all the peaks relevant to iPS are absent, giving a lower crystallinity as shown in Fig. 7(b). On the basis of the nucleation theories, a larger thickness of lamellae is required to stabilize lamellar nuclei and the nucleation density is lower when samples are crystallized at a lower degree of supercooling (higher T_c). Thus, the absence of subsequent iPS crystallization at 200 °C is plausibly attributed to the difficulties in forming stable lamellar nuclei when the size of the segregated domains is commensurate with the lamellar thickness of iPS. Moreover, it should be noted that the effective nucleation density of iPS in the segregated domains becomes diminished at high T_c.

Table 4
Two-step melt-crystallization data for the iPS component in sPS/iPS blends at 250 °C/T_{c2}, together with results of the neat iPS at T_{c2}

T_{c2} (°C)	iPS in the blends		Neat iPS	
	k (min^{-1})	n	k (min^{-1})	n
200	NO	NO	2.03×10^{-4}	1.7
175	8.48×10^{-5}	2.3	2.67×10^{-4}	2.0
150	1.30×10^{-5}	2.3	5.17×10^{-5}	1.8

sPS in the blends: $k=0.11$ min^{-1}, $n=2.3$ at 250 °C.

3.5. Crystal growth rates

Studies of the influence of iPS (aPS) on the sPS crystal growth rate would also provide useful information on the blend miscibility. The crystal growth rate is closely related to the degree of supercooling ΔT ($=T_m^0-T_c$, where T_m^0 is the equilibrium melting temperature). As shown in Fig. 8, T_m exhibited a linear dependence on crystallization temperature, following the Hoffman–Weeks relationship. The lower melting peak is more appropriate for T_m^0 analysis when double-melting is detected. Extrapolation of the plot to the line $T_m=T_c$ enabled the T_m^0 to be determined. The deduced T_m^0 for the neat sPS and iPS are 290.8 and 241.7 °C, respectively, which are comparable with those obtained previously [9,10] (Table 1). Moreover, T_m^0 of the sPS component in the blends remains unchanged regardless of the addition of iPS or aPS since the interaction parameter in the sPS/aPS and sPS/iPS pairs is null. Thus, blending of sPS with aPS (or iPS) provides appropriate models for studying athermal blend systems. Effect of the aPS molecular weight, which alters the entropy effect alone, on the sPS crystallization behavior is currently in progress and will be the subject of a future article.

Fig. 9 shows the T_c-temperature and ΔT-dependence of G for neat sPS, neat iPS, sPS/aPS = 5/5 and sPS/iPS = 5/5 blends. Addition of iPS (aPS) depresses the spherulitic growth rate of sPS. However, superposition of the growth rates of the sPS blends with neat sPS is evident when G is normalized with the sPS content (Fig. 9(b)). Compared with sPS/aPS blends, the more scattered results of sPS/iPS blends may be attributed to the phase separation event. Based on the Lauritzen–Hoffman

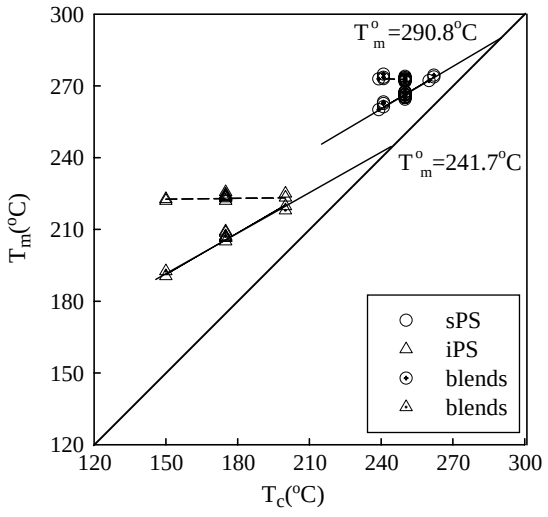

Fig. 8. Hoffman–Weeks plots to determine the equilibrium melting temperatures of iPS and sPS.

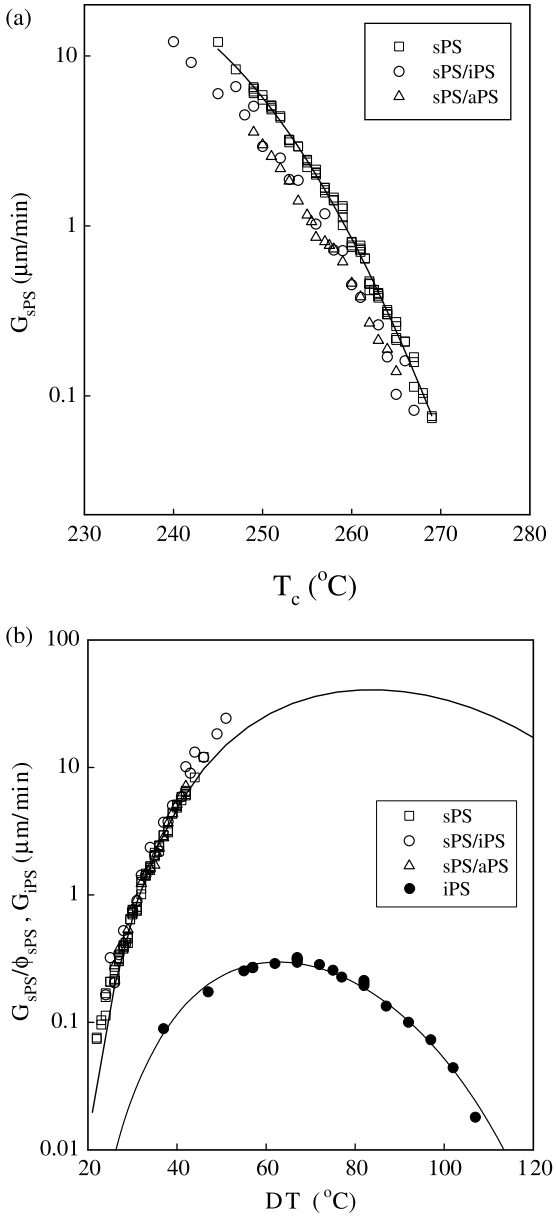

Fig. 9. (a) T_c-dependence, and (b) supercooling dependence of growth rates of neat sPS, iPS, and blends of sPS/iPS and sPS/aPS. (ϕ_{sPS} is the volume fraction of sPS).

theory [29–31], the derived growth equations for the sPS and iPS are given in Eqs. (2) and (3) and the solid lines in Fig. 9(b) are both fits with these equations (the unit of T_c in K).

$$G_{sPS}(T_c) = 255,480 \exp\left[\frac{-661.9}{T_c - 342}\right] \exp\left[\frac{-146,400}{\Delta T T_c f}\right] \quad (2)$$

$$G_{iPS}(T_c) = 17,450 \exp\left[\frac{-785.1}{T_c - 333}\right] \exp\left[\frac{-116,620}{\Delta T T_c f}\right] \quad (3)$$

The first exponential term is related to the temperature-dependence of the chain mobility and is expressed by:exp[$-\Delta E_{WLF}/(R(T_c - T_\infty))$] where ΔE_{WLF} is the Williams–Landel–Ferry (WLF) type activation energy for chain diffusion, R is the gas constant and T_∞ is the critical temperature below which the motion of polymer chains is ceased. T_∞ is usually lower than the T_g and is expressed as $T_g - C$, where C is a constant depending on the polymer, being 30 and 26 K for iPS and sPS, respectively. The derived ΔE_{WLF} values for iPS and sPS are 1560 and 1315 cal/mol, respectively [32,33]. The second exponential term is associated with the nucleation process and generally given by: exp[$(-2b_0\sigma\sigma_e T_m^0)/(k\Delta H_f \Delta T T_c f)$] for regime II growth which is found valid for iPS and sPS [8,29], where b_0 is the crystal layer thickness, ΔH_f is the heat of fusion, f is a corrected factor, and σ and σ_e are the surface free energy for the lateral and fold surface, respectively. The derived parameters in constructing the predicted solid lines in Fig. 9(b) are given in Table 5. Due to the interplay between the chain mobility and nucleation barrier, growth rate of sPS reaches a maximum value of 40.57 μm/min as shown in Fig. 9(b) at $\Delta T = 86$ °C, corresponding to $T_c = 205$ °C. For iPS, a maximum G of 0.30 μm/min is observed at $\Delta T = 62$ °C with a T_c of 180 °C, which is consistent with previous findings [34]. The pre-factor, G_0, is relevant with the structure, tacticity and molecular weight (MW) of the polymer studied. It is of interest to note that the growth rate of sPS is ca. at least one order of magnitude higher than that of iPS at a given ΔT [35]. Moreover, the activation energy for chain mobility and the fold surface free energy are relatively lower for sPS. It has been pointed out that G_0 is dependent on the MW of polymers and a weak function for iPS has been derived: $G_0 \sim MW^{-0.25}$ [34]. For a fair comparison, the corresponding G_0 value for iPS with a MW of $\sim 2\times10^5$ is calculated to be 20,800 μm/min, which is still about one order of magnitude lower than the sPS at the given MW. Hence, in contrast with sPS, the significant reduction of the iPS growth rate is attributed to the lower G_0 value as well as the relatively higher values of σ_e and ΔE_{WLF}.

3.6. Lamellar and segregation morphology

Due to the large difference in the crystal growth rate between iPS and sPS at a given T_c as shown in Fig. 9(b), it was concluded that crystallization of sPS is eventually complete before the crystallization of iPS starts. In other words, the crystallization of iPS takes place in the segregated domains, resulting from the rejection of amorphous iPS diluent (also

Table 5
Kinetics results used for the growth rate prediction for sPS and iPS

	T_g (°C)	T_m^0 (°C)	ΔE_{WLF} (cal/mol)	b_0 (nm)	ΔH_f (J/cm^3)	σ (erg/cm^2)	σ_e (erg/cm^2)	G_0 (μm/min)
sPS	95	291	1315	1.44	87.9	9.9	11.1	255,480
iPS	90	242	1560	0.63	91.1	6.6	33.7	17,450

some uncrystallizing sPS chains) during sPS crystallization. Depending on the relative distance and location where amorphous iPS are expelled and reside, three distinct segregated morphologies are defined, i.e. interlamellar (IL), interfibrillar (IF) and interspherulitic (IS) segregation. Based on the SEM micrographs as shown in Fig. 10, IF segregation of iPS component is evident after sPS crystallization is concluded. The length and width of the segregated iPS domains are typically ca. 790–800 and 150–170 nm, respectively, independent of the T_c at which crystallization of sPS takes place.

One-step crystallization from the melt to 175 °C generated two separate lamellar stack domains, as shown in Fig. 11(a) observed by TEM, where the relatively lighter regions are for iPS lamellar stacks possessing a higher density than sPS lamellar stacks. Within the spherulites, a wavy characteristics of lamellar growth is observed in contrast with the neat sPS, exhibiting straight growth habit. It is also noted that the lamellar thicknesses of sPS and iPS are similar and the growth direction of iPS lamellae is parallel to the already-formed sPS lamellar stacks. Fig. 11(b) shows the morphology of sPS/iPS

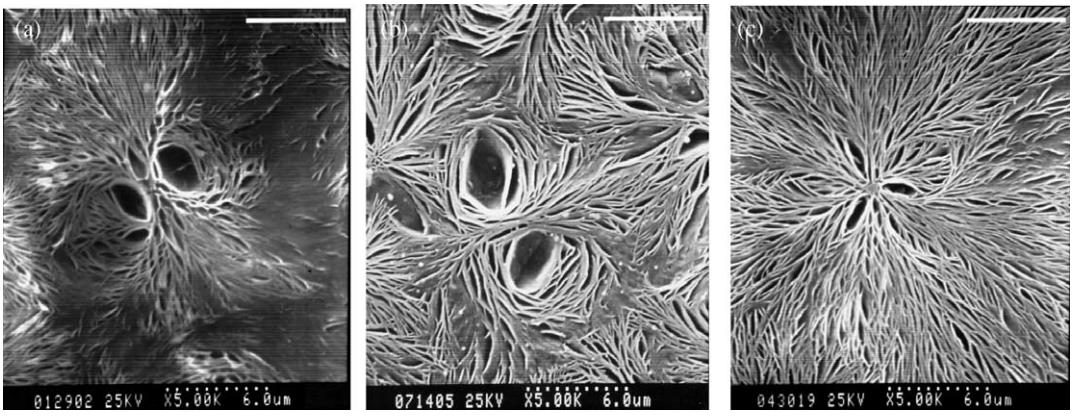

Fig. 10. SEM images of sPS/iPS blends quenched to room temperature after sPS crystallization at various T_c to reveal the placement of iPS, (a) 241 °C, (b) 250 °C, and (c) 262 °C. Scale bar: 6 μm.

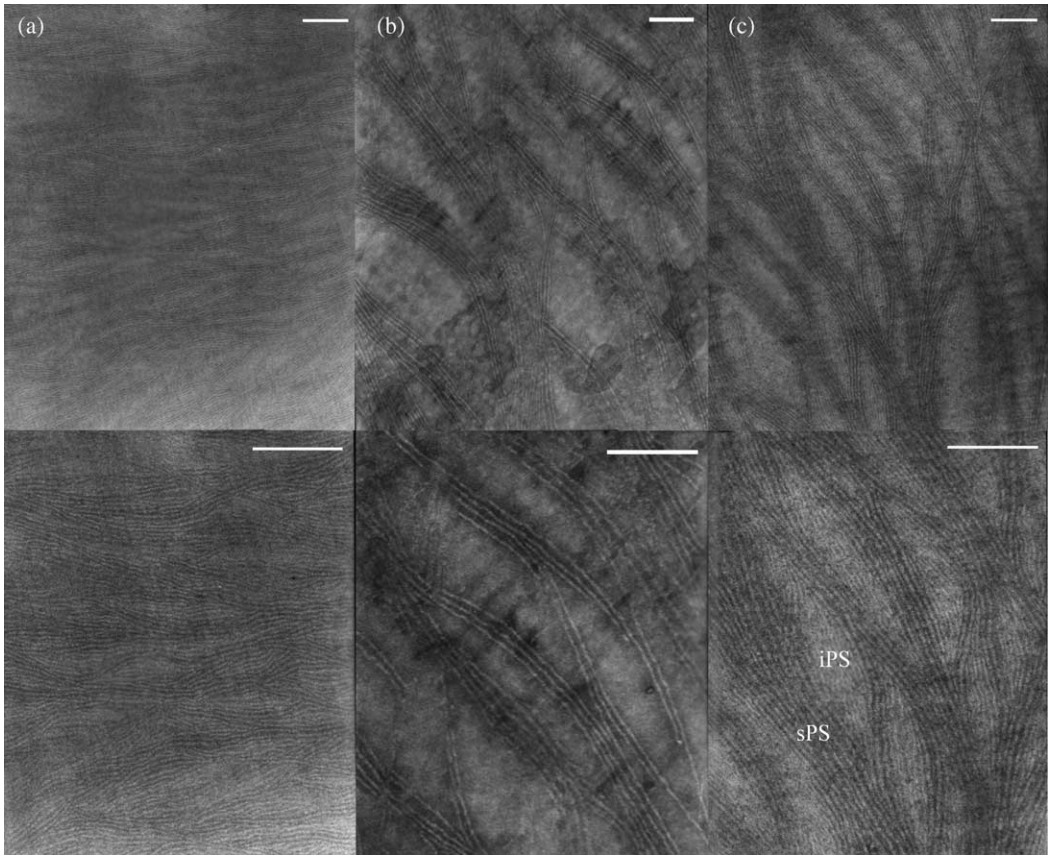

Fig. 11. TEM images of sPS/iPS = 5/5 (a) melt-crystallized at 175 °C, (b) melt-crystallized at 250 °C and then quenched to room temperature, (c) 250/175 °C two-step crystallization. Scale bar: 200 nm.

after the temperature drop from 300 to 250 °C where only sPS can crystallize. It is evident that sPS lamellar stacks are developed and the uncrystallized iPS forms the isolated domains between the sPS stacks, in agreement with SEM images as shown in Fig. 10(b). Subsequent crystallization of iPS upon cooling to 175 °C will take place in these interfibrillar regions as shown in Fig. 11(c). The iPS lamellae are packed parallel to the pre-existing sPS lamellar stacks. For the 250/200 °C two-step crystallization, on the other hand, a lamellar morphology similar with Fig. 11(b) is observed, indicating the absence of iPS lamellae and giving rise to the crystalline/amorphous blends. Thus, the subsequent crystallization of iPS may not commence at high T_c due to the nucleation difficulties in forming stable lamellar nuclei in the confined space. It seems that the relative dimensions of the segregated domains and the critical lamellar thickness is a crucial factor in determining the crystallization of iPS in such constrained regions.

Our previous morphological studies on the sPS/aPS blends showed that interfibrillar segregation of aPS component occurs during sPS crystallization [8]. Moreover, Warner et al. [11] have studied the small-angle X-ray scattering of iPS/aPS blends and shown that the long period of iPS lamellar stacks remains unchanged upon addition of aPS component. They concluded that the amorphous aPS is trapped in the interfibrillar regions within iPS spherulites. Combined with present studies on the sPS/aPS and sPS/iPS blends, it seems that interfibrillar segregation of the amorphous component is the predominant morphology for polystyrene blends with different tacticity.

4. Conclusion

To detect the subtle phase variation in the blends where the structure of individual components is similar, such as sPS/aPS and sPS/iPS blends, conventional DSC and OM techniques might be inadequate due to the T_g proximity and low phase contrast between phases. In this study, enthalpy relaxation is proven quite applicable to provide the evidence of phase separation of the sPS/iPS blends due to the presence of two recovery peaks together with two exotherms associated with sPS crystallization in the respectively-separated two phases. It is further supported by the bi-continuous phase-separated structure observed by phase contrast microscopy and SEM as well. On the other hand, both sPS and aPS show completely miscible in the melt. Crystal growth rates of sPS in the sPS/aPS and sPS/iPS blends are found to reduce mainly due to the dilution effect regardless of the phase structure prior to crystallization. For sPS/iPS blends, co-crystallization of both components into the same lattice is not expected to take place due to the large differences in crystallization rate. Depending on the thermal treatments, however, sPS possesses various crystal forms when crystallized from the melt or glassy states.

For sPS/iPS blends, the observation of two melting transitions corresponding to those of the constituents and the lamellar morphologies revealed by TEM suggest that crystallization takes place separately in the blends at the length scale of lamellae, and lamellae of sPS and iPS coexist within the same spherulites. Crystallization of iPS mainly takes place in the interfibrillar regions between sPS lamellar stacks, which have been crystallized already. Moreover, depending on the segregated domain size and the lamellar thickness, crystallization of iPS might be prohibited when the initial lamellae are too thick at a given supercooling to be nucleated in the confined domains. Thus, the crystallizability of iPS is dependent upon the relative dimensions of the segregated domains and iPS lamellar thickness. For sPS/aPS blends [8], segregation of rejected amorphous aPS during sPS crystallization was evidently observed from TEM images which showed aPS pockets located between sPS lamellar stacks, leading to the interfibrillar segregation as well.

Acknowledgements

The authors are grateful to the National Science Council of Taiwan (ROC) for the research grant (NSC91-2216-E-006-031) that supported this work. Part of this work was presented at the World Polymer Congress (MACRO2004) and the authors thank the National Science Council for the support of their trip (93-2914-I-006-064-A1) to Paris, France.

References

[1] Xu G, Clancy TC, Mattice WL, Kumar SK. Macromolecules 2002;35:3309.
[2] Bonnet M, Buhk M, Trogner G, Togausch KD, Petermann J. Acta Polym 1998;49:174.
[3] Hong BK, Jo WH, Kim J. Polymer 1998;39:3753.
[4] Woo EM, Wu FS. J Polym Sci, Polym Phys Ed 1998;36:2725.
[5] Chiu FC, Peng CG. Polymer 2002;43:4879.
[6] Park JY, Kwon MH, Park OO. J Polym Sci, Polym Phys Ed 2000;38:3001.
[7] Wang C, Liao WP, Cheng YW, Lin TL. Polymer 2004;45:961.
[8] Wang C, Liao WP, Wang ML, Lin CC. Polymer 2004;45:973.
[9] Wang C, Hsu YC, Lo CF. Polymer 2001;42:8447.
[10] Wunderlich B. Macromolecular physics. vol. 1. New York: Academic Press, Inc.; 1973 p. 388.
[11] Warner FP, MacKnight WJ, Stein RS. J Polym Sci, Polym Phys 1977;15:2113.
[12] Wang C, Chen CC, Cheng YW, Liao WP, Wang ML. Polymer 2002;43:5271.
[13] Kit KM, Schultz JM. J Polym Sci, Polym Phys Ed 1998;36:873.
[14] Bosma M, ten Brinke G, Ellis TS. Macromolecules 1988;21:1465.
[15] Cowie JMG, Ferguson R. Macromolecules 1989;22:2307.
[16] Xu H, Ince BS, Cebe P. J Polym Sci, Polym Phys Ed 2003;41:3026.
[17] Auriemma F, Petraccone V, Dal Poggetto F, De Rosa C, Guerra G, Manfredi C, et al. Macromolecules 1993;26:3772.
[18] Nakaoki T, Kobayashi M. J Mol Struct 2003;655:343.
[19] Guerra G, Vitagliano VM, De Rosa C, Petraccone V, Corradini P. Macromolecules 1990;23:1539.
[20] Chatani Y, Shimane Y, Ijitsu T, Yukinari T. Polymer 1993;34:1625.
[21] Woo EM, Sun YS, Yang CP. Prog Polym Sci 2001;26:945.
[22] Bu W, Li Y, He J, Zeng J. Macromolecules 1999;32:7224.
[23] Li Y, He J, Qiang W, Hu X. Polymer 2002;43:2489.
[24] Sun YS, Woo EM. Macromolecules 1999;32:7836.
[25] De Rosa C, De Ballesteros OR, Di Gennaro M, Auriemma F. Polymer 2003;44:1861.
[26] Hong BK, Jo WH, Lee SC, Kim J. Polymer 1998;39:1793.
[27] Petraccone V, Auriemma F, Dal Poggetto F, De Rosa C, Guerra G, Corradini P. Makromol Chem 1993;194:1335.
[28] Liu J, Petermann J. Polymer 2001;42:6453.

[29] Hoffman JD, Davis GT, Lauritzen JI. In: Hannary NB, editor. Treatise on solid state chemistry. New York: Plenum Press; 1976 [Chapter 7].
[30] Hoffman JD, Miller RL. Polymer 1997;38:3151.
[31] Hoffman JD, Miller Rl, Marand H, Roitman DB. Macromolecules 1992; 25:2221.
[32] Suzuki T, Kovacs AJ. Polym J 1970;1:82.
[33] Based on the approach proposed by Suzuki and Kovacs [32], values of ΔE_{WLF} and C for neat sPS are derived from the best fits of spherulitic growth rate results at low crystallization temperatures (115–150 °C) obtained by small-angle light scattering. In this crystallization range, polarized optical microscopy becomes infeasible to apply due to the small sPS spherulites developed. This part of experimental results will be presented in a future article.
[34] Lemstra PJ, Postma J, Challa G. Polymer 1974;15:758.
[35] Cimmino S, Pace ED, Martuscelli E, Silvestre C. Polymer 1991;32: 1080.